

SUPPORTING INFORMATION

Exclusions for neuroimaging scan

Out of 237 youths who participated in the SAND study at baseline, 16 declined to participate in MRI scanning, 3 exceeded MRI table weight limit, 1 reported a medical restriction, 7 had braces or other metal in body, 1 had a risk of pregnancy, and 2 were excluded for diagnosis of Autism Spectrum Disorder. After these exclusions, of 207 youths who participated in MRI scanning, 5 did not finish scan, 6 had significant artifacts in structural anatomical MRI data, 5 was excluded for significant motion artifacts in the functional data, and 17 had accuracy below 70% on fMRI task. The final sample used for time-series extraction and subsequent analyses was 174. See Figure S1 for illustration.

MRI data acquisition and preprocessing

MRIs were acquired using 3T GEDiscovery MR750 scanner with 8-channel head coil. Head padding and instructions limited movement. T1-weighted gradient echo images were first captured (TR=12ms, TE=5ms, TI=500ms, flip angle=15°, FOV=26cm, slice thickness=1.44mm, 256x192 matrix, 110 slices). fMRI T2*-weighted blood oxygenation level dependent (BOLD) images were then captured using reverse spiral sequence (Glover & Law, 2001) of 40 contiguous axial 3mm slices (TR=2000ms, TE=30ms, flip angle=90°, FOV=22cm, voxel size=3.44x3.44x3mm, ascending acquisition, parallel to AC-PC line). Anatomical images were skull-stripped ($f=.25$) using Brain Extraction Tool (BET) in FSL version 6.0 (Jenkinson et al., 2012) and segmented into gray matter, white matter, and cerebrospinal fluid using FSL FAST. After large temporal spikes in the k-space functional data ($>2 SD$) were removed, field maps

were corrected and functional images were reconstructed using MATLAB. Noise from cardiac and respiratory motion were removed using RETROICOR and slice-timing correction using SPM8 (Wellcome Department of Cognitive Neurology, London, UK; <http://www.fil.ion.ucl.ac.uk>). Moreover, first ten volumes of functional data were removed to ensure the stability of signal intensity. Following these steps, the functional data were further preprocessed using FSL fMRI Expert Analysis Tool (FEAT). Functional images were skull-stripped and spatially smoothed using FSL FMRIB's Automated Segmentation Tool (Woolrich et al., 2001), and registered to subject-specific previously skull-stripped and segmented anatomical images. Motion correction was performed using MCFLIRT and spatial smoothing using a Gaussian kernel of FWHM 6.0mm was applied. Grand-mean intensity of the entire 4D dataset was normalized by a single multiplicative factor and FSL motion outliers were ran to extract framewise displacement motion parameters (Power et al., 2012). ICA-AROMA was used to remove motion-related artifacts in the data, nuisance signal derived from white matter and cerebrospinal fluid were regressed out, and data with signal below 0.01Hz were then high-pass filtered. These preprocessing steps were applied using detailed scripts (Adriene M. Beltz et al., 2019) that were also utilized in previous investigation (Goetschius, Hein, McLanahan, et al., 2020).

fMRI task paradigm

Neuroimaging data was collected using event-related emotion (faces) task (see Figure S2 for visual representation of task paradigm design). Participants were shown a series of emotional faces (Tottenham et al., 2009) and indicated if they were viewing a female or male face. Gender (female, male), race (European American, African American), and emotion (fearful, happy, sad,

neutral, angry) of the actor were counterbalanced and randomly presented across 100 trials. Each trial consisted of a fixation cross (500ms) followed by 250ms of an emotion stimuli, then 1500ms of blank screen during which participants are expected to respond using button press. Functional data from each participant across all trials of emotion task (without any contrasting) were extracted for subsequent processing.

ROI selection and data extraction

The present investigation focused on seven bilateral regions that have been shown to be implicated in processes related to anxiety and depression: amygdala, anterior cingulate cortex, dorsomedial prefrontal, insula, orbitofrontal, subgenual cingulate, and ventral striatum. The amygdala has most commonly been linked to salience and fear processing (Davis, 1992; Janak & Tye, 2015), and amygdala function has been widely found to be implicated in anxiety and depression (Davidson, 2002; Rauch et al., 2003; Thomas et al., 2001; Whalen et al., 2002). Similarly, the anterior cingulate cortex has been found to be substantially involved in processes relating to affective and mood disorders (Drevets et al., 2008; Greicius et al., 2007; Margulies et al., 2007; Stevens et al., 2011). Most prominently, evidence from clinical trials demonstrates that deep brain stimulation of the subgenual cingulate can reduce depressive symptoms (Mayberg et al., 2005), suggesting the importance of this region in mood disorders. Both the dorsomedial and orbitofrontal cortex are believed to be implicated in emotion regulation and higher-order processing. Evidence has shown that disruption in brain function within these regions is important in affective disorders (Drevets, 2007; Eickhoff et al., 2016; Moses-Kolko et al., 2010). The insula is another important region for salience processing (Menon & Uddin, 2010; Uddin, 2015) and the bidirectional communication between insula and dorsal anterior cingulate cortex

has been linked to anxiety disorders in both clinical and non-clinical populations (Klumpp et al., 2012, 2013). Finally, the ventral striatum is central to reward processing and reward-based learning (Pagnoni et al., 2002; Schultz et al., 1992), which are important features of depressive and affective disorders (Robinson et al., 2012).

Consistent with our previous investigation (Goetschius, Hein, McLanahan, et al., 2020), ROI coordinates were extracted from NeuroSynth (Yarkoni et al., 2011) (<https://neurosynth.org/analyses/>) and preregistered (<https://osf.io/tgj3s/>). NeuroSynth is a meta-analytic tool that combines results from published neuroimaging articles using an automated parser. Findings from published articles are tagged with a specific term to produce a statistical inference maps for activation maps associated with tagged keywords. Specific ROI names (i.e., “amygdala”, “anterior cingulate”, “dorsomedial”, “insula”, “orbitofrontal”, “subgenual”, “ventral striatum”) were used as keywords to search for peak activity on the NeuroSynth website and corresponding association maps were then downloaded. Voxel coordinates from downloaded images were subsequently extracted using FSL and then utilized to create an ROI 8mm-diameter sphere using fslmaths. To ensure that there were no significant differences in functional data driven by sphere size, functional data were extracted from one ROI (i.e., left and right amygdala) using 6.5mm-radii sphere that were previously used in prior investigation (Goetschius, Hein, McLanahan, et al., 2020), and extracted data were compared with data extracted using 8mm-diameter sphere used in present investigation. There were no significant differences between the two, and results can be found in Table S9.

Measures for anxiety and depressive symptoms

Anxiety at wave 1 and wave 2 was measured using the 38-item Screen for Anxiety Related Disorders (Birmaher et al., 1997) (Cronbach's $\alpha = .92$ at wave 1; Cronbach's $\alpha = .95$ at wave 2). Anxiety at wave 3 was measured using the 21-item Beck Anxiety Inventory (Beck et al., 1988) (Cronbach's $\alpha = .95$). Depression at wave 1 and wave 2 was measured using the Mood and Feelings Questionnaire (Angold et al., 1995) 34 items at wave 1, 30 items at wave 2) (Cronbach's $\alpha = .91$ at wave 1; Cronbach's $\alpha = .96$ at wave 2). Depression at wave 3 was measured using the 20-item Beck Depression Inventory (Beck et al., 1996) (Cronbach's $\alpha = .91$).

Covariates

Sex was parent-report at child age 1 (0 = female, 1 = male). Pubertal development was measured at wave 1 by youth report on the Pubertal Development Scale (Petersen et al., 1988) that measured changes in child height, body hair, skin, facial hair and voice (males only), breast development and menarche (females only). Responses were coded on 4-point scale: 1 = no development to 4 = completed development; and score was a sum of all items endorsed. Ethnoracial identity was self-identified by youth at age 15 (wave 1): Black, non-Hispanic; white, non-Hispanic; Hispanic or LatinX; and Other. In cases where youth did not identify race/ethnicity ($n = 8$), parent report of race/ethnicity was utilized. Three dummy-coded variables were created to represent ethnoracial identity with Black as the reference variable. Annual household income was reported by primary caregiver at wave 1. If caregiver did not report annual household income, income was determined by other caregiver's report who are cohabitating with child. In the case that neither caregivers reported income, annual income was imputed by regression-based imputation. Framewise displacement was computed in FSL as a measure of in-scanner motion by averaging differences in rotation and translation parameter

(Power et al., 2012). Early adverse experiences (i.e., violence exposure, social deprivation) were included as covariates to account for early childhood experiences that may relate to neurobiological development as found by previous investigation using this sample (Goetschius, Hein, McLanahan, et al., 2020; Goetschius, Hein, Mitchell, et al., 2020; Hein et al., 2020; Peckins et al., 2020). Both violence exposure and social deprivation were measured using composite scores of exposure at ages 3, 5, and 9. Violence exposure was based on: (1) parent responses on child physical and emotional abuse questions in the Parent-Child Conflict Tactics Scale (Straus et al., 1998); (2) child exposure to neighborhood violence; (3) maternal report of intimate partner violence. Social deprivation was based on: (1) parent report on physical and emotional neglect on the Parent-Child Conflict Tactics Scale (Straus et al., 1998); (2) neighborhood cohesion. For both measures, scores were first standardized and z-scores across each dimension of early adversity (violence exposure; social deprivation) across each timepoint were summed. Cognitive abilities (i.e., reading comprehension, mathematical abilities) were measured at age 9 using the Passage Comprehension and Applied Problems subtests taken from then Woodcock Johnson test (Woodcock et al., 2001). Passage Comprehension involves matching symbolic pictures to word representation as well as reading a passage and identifying missing words in the passage. The items progressively become more difficult by increasing passage length and complexity of vocabulary, syntactic, and semantic cues. Applied Problems subtest involves solving math problems, which increases in difficulty with item level. Child's percentile rank was used for both subtests. Cohabitation status was self-reported at wave 3 (during the pandemic). Participants reported whether they are living with spouse, partner or girlfriend/boyfriend during the pandemic (1 = yes, 0 = no). Similarly, parental status was self-reported at wave 3. Participants reported whether they are living with biological, step, adopted or

foster children during the pandemic (1 = yes, 0 = no). All continuous variables were mean-centered for further statistical analyses.

S-GIMME

S-GIMME begins with a null model. First, group-level connections are added for everyone if they significantly improve model fit for at least 75% of the sample as assessed by the Lagrange Multiplier tests (Gates et al., 2010). Individuals are then classified into subgroups using a Walktrap community detection algorithm (Gates et al., 2017), allowing for an unsupervised model search that reflects personalized network without averaging across individuals. Subgroup-level connections are then added for everyone in a given subgroup if they significantly improve models for at least 51% of individuals within each subgroup. Lastly, individual-level connections (i.e., connections unique for each person) are added until individual model well-fit the observed data. After person-specific networks were generated, contemporaneous edges were extracted for subsequent analyses, consistent with previous investigations (Goetschius, Hein, McLanahan, et al., 2020) as lagged connections are amenable to hemodynamic temporal dependencies (Gates et al., 2010; Smith, 2012). See Figure S3 for an illustration of S-GIMME process.

Robustness checks for functional connectivity estimation

To establish reliability in the functional data, split-half reliability test was performed by applying S-GIMME separately to odd and even volumes of the data (Elliott et al., 2021; Pronk et al., 2022). Results show good correspondence between the resulting subgroups. Two subgroups emerged from analyses of both datasets with high correspondence in subgroup membership and connectivity (subgroups did not differ across runs: $\chi^2(1) = 0.299, p = .585; r = .83, p < .001$ for

subgroup A path count; $r = .82$, $p < .001$ for subgroup B path count) (Table S10). Anxiety and depressive symptoms for each subgroup did not differ between the datasets (Subgroup A Anxiety: $t(90) = .360$, $p = .720$; Depression: $t(92) = -.034$, $p = .973$; Subgroup B Anxiety: $t(144) = -.331$, $p = .741$; Depression: $t(142) = -.047$, $p = .963$). Furthermore, to establish robustness in functional connectivity estimation for the sample, S-GIMME was applied to five randomly drawn subsamples (80%, sampled with replacement; $N=139$). Consistent with original results, two subgroups were derived with good correspondence in subgroup membership and connectivity between all five subsamples and the full sample (Table S11; Figure S5).

Robustness checks in predictive models

Several robustness checks were performed to all models. First, models were re-examined without inclusion of subjects that had standardized network model psi values of above 1 ($N=18$ for subgroup A; $N=20$ for subgroup B), which would reflect greater than 100% unexplained variation for an ROI in the model – an impossible value that could reflect model overfitting (Lütkepohl, 2005). Next, model residuals were examined and any influential outliers identified using Cook's distance were excluded in subsequent models for sensitivity checks. Finally, sensitivity analyses were performed to account for covariates that may explain variance in the outcome (i.e., age, sex, pubertal development, ethnoracial identity, annual household income, days since study commenced) and additional covariates (i.e., scanner framework displacement, violence exposure, social deprivation, reading comprehension, mathematical abilities, residential status with partner during pandemic, residential status with child during pandemic).

Comparison network

1 To ensure that the results pertained to hypothesized ROIs we selected based on theory, functional
 2 connectivity network was estimated from a set of comparison ROIs (7 nodes from each
 3 hemispheres) related to visual, auditory, motor, and language processing that were hypothesized
 4 to be unrelated to susceptibility to anxiety and depression. Similar procedures were utilized to
 5 obtain ROI coordinates: specific terms were used as keywords in NeuroSynth (i.e., “audio”,
 6 “fusiform”, “language”, “sensor”, “supplementary motor area”, “visual”); corresponding voxel
 7 coordinates were then extracted and then utilized to create an 8mm-diameter ROI sphere using
 8 fslmaths (see Table S3 for MNI coordinates of ROIs in comparison network). These ROIs were
 9 then registered to subject-specific anatomical images and time-series data extracted for S-
 10 GIMME processing. S-GIMME arrived at a 2-subgroup solution, but results showed that there
 11 were no statistically significant differences in anxiety or depression between the two subgroups
 12 in the comparison network (anxiety: $\beta=.053$, $p=.490$; depression: $\beta=.059$, $p=.438$). Furthermore,
 13 no significant subgroup-adversity interaction was found in relation to anxiety ($\beta=.054$, $p=.630$)
 14 or depression ($\beta=.148$, $p=.188$) during the pandemic. Results from comparison network analyses
 15 are reported in Table S4.

1 **Table S1.** Full and included sample comparisons ^a

	Full sample (N=237)	Wave 1 (baseline) sample (N=174)
Age (years)	$M = 15.87 \mid SD = 0.54$	$M = 15.86 \mid SD = 0.53$
Sex	F = 124 (52.3%) M = 113 (47.7%)	F = 94 (54.0%) M = 80 (46.0%)
Ethnoracial identity	Black = 181 (76.4%)	Black = 133 (76.4%)
	White = 32 (13.5%)	White = 21 (12.1%)
	Hispanic/LatinX = 13 (5.5%)	Hispanic/LatinX = 12 (6.9%)
	Other/Multiracial = 11 (4.6%)	Other/Multiracial = 8 (4.6%)
Annual Income	<\$15,000 = 57 (24.1%)	<\$15,000 = 41 (23.6%)
	\$15,000-39,999 = 70 (29.5%)	\$15,000-39,999 = 49 (28.2%)
	\$40,000-69,999 = 58 (24.5%)	\$40,000-69,999 = 40 (23.0%)
	>\$70,000 = 51 (21.5%)	>\$70,000 = 43 (24.7%)
	Missing/Not reported = 1 (0.4%)	Missing/Not reported = 1 (0.6%)
	Wave 2 sample (N=128)	Wave 3 (COVID-19) (N=119)
Age (years)	$M = 15.85 \mid SD = 0.54$	$M = 15.87 \mid SD = 0.54$
Sex	F = 77 (60.6%) M = 51 (40.2%)	F = 74 (62.2%) M = 45 (37.8%)
Ethnoracial identity	Black = 92 (71.9%)	Black = 83 (69.7%)
	White = 18 (14.1%)	White = 19 (16.0%)
	Hispanic/LatinX = 11 (8.6%)	Hispanic/LatinX = 10 (8.4%)
	Other/Multiracial = 7 (5.5%)	Other/Multiracial = 7 (5.9%)
Annual Income	<\$15,000 = 25 (19.5%)	<\$15,000 = 27 (22.7%)
	\$15,000-39,999 = 31 (24.2%)	\$15,000-39,999 = 28 (23.5%)
	\$40,000-69,999 = 34 (26.6%)	\$40,000-69,999 = 26 (21.8%)
	>\$70,000 = 38 (29.7%)	>\$70,000 = 37 (31.1%)
	Missing/Not reported = 0 (0%)	Missing/Not reported = 1 (0.8%)

2 ^a Samples did not differ in age: $F(3,654)=.038, p=.99$; sex: $F(3,654)=1.44, p=.229$; race:3 $F(3,654)=.10, p=.959$; annual income: $F(3,651)=1.19, p=.311$;

4

5 **Table S2.** MNI coordinates of individual Regions of Interest (ROI)

Hemisphere	Regions of Interest (ROI)	MNI coordinates
<i>Left</i>	Amygdala	-18, -6, -20
	Dorsal anterior cingulate cortex	-10, 26, 26
	Dorsomedial prefrontal cortex	-16, 46, 36
	Insula	-34, 22, 0
	Orbitofrontal prefrontal cortex	-10, 38, -18
	Subgenual cingulate cortex	-10, 22, -16

	Ventral striatum	-10, 10, -6
<i>Right</i>	Amygdala	18, -6, -20
	Dorsal anterior cingulate cortex	10, 26, 26
	Dorsomedial prefrontal cortex	16, 46, 36
	Insula	34, 22, 0
	Orbitofrontal prefrontal cortex	10, 38, -18
	Subgenual cingulate cortex	10, 22, -16
	Ventral striatum	10, 10, -6

1

2 **Table S3.** MNI coordinates of ROIs in comparison network

<i>Hemisphere</i>	<i>NeuroSynth key terms</i>	<i>MNI coordinates</i>
<i>Left</i>	Audio	-50, -18, 6
	Fusiform	-42, -50, -20
	Language	-56, -42, 4
	Language	-46, 16, 22
	Sensorimotor	-36, -20, 54
	Supplementary motor area	-5, -6, 60
	Visual	-46, 70, 2
<i>Right</i>	Audio	50, -18, 6
	Fusiform	42, -50, -20
	Language	56, -42, 4
	Language	46, 16, 22
	Sensorimotor	36, -20, 54
	Supplementary motor area	5, -6, 60
	Visual	46, 70, 2

3

4 **Table S4.** Results from predictive models using comparison network

	Change in anxiety		Change in depression	
	β	p	β	p
Subgroup	0.026	0.706	0.053	0.490
Initial symptoms	-0.451	<.001	-0.091	0.236
	$F(2,170)=22.02, p<.001$		$F(2,170)=1.01, p=.366$	

5

	Anxiety at wave 3		Depression at wave 3	
	β	p	β	p
Subgroup	-0.102	0.243	-0.107	0.219
COVID-19 adversity	0.147	0.003	0.268	0.018
Subgroup x COVID-19 adversity	0.054	0.630	0.149	0.188
	$F(3,114)=6.52, p<.001$		$F(3,114)=6.66, p<.001$	

6

1 **Table S5.** Node centrality for each subgroup

<i>Hemisphere</i>	<i>Node</i>	<i>Subgroup A</i>		<i>Subgroup B</i>		<i>t-test results¹</i>
		<i>Mean</i>	<i>SD</i>	<i>Mean</i>	<i>SD</i>	
<i>Left</i>	Amygdala	.123	.033	.101	.042	$t(170.72)= 3.93$, $p<.001$, $p\text{-adjust}=.002$
	Dorsal anterior cingulate cortex	.131	.043	.159	.047	$t(171.32)= -4.09$, $p<.001$, $p\text{-adjust}<.001$
	Dorsomedial prefrontal cortex	.152	.043	.172	.051	$t(172)= -2.75$, $p=.007$, $p\text{-adjust}= .092$
	Insula	.141	.044	.164	.048	$t(171.14)= -3.28$, $p=.001$, $p\text{-adjust}= .017$
	Orbitofrontal prefrontal cortex	.147	.041	.161	.038	$t(163.08)= -2.33$, $p=.021$, $p\text{-adjust}= .298$
	Subgenual cingulate cortex	.153	.040	.144	.042	$t(170)= 1.43$, $p=.155$, $p\text{-adjust}= 2.164$
	Ventral striatum	.162	.043	.108	.043	$t(167.23)= 8.17$, $p<.001$, $p\text{-adjust}<.001$
<i>Right</i>	Amygdala	.102	.044	.107	.048	$t(171.16)= -.80$, $p=.426$, $p\text{-adjust}= 5.968$
	Dorsal anterior cingulate cortex	.158	.040	.154	.045	$t(171.89)= .74$, $p=.460$, $p\text{-adjust}= 6.434$
	Dorsomedial prefrontal cortex	.117	.047	.130	.053	$t(171.5)= -1.66$, $p=.099$, $p\text{-adjust}= 1.383$
	Insula	.156	.037	.184	.051	$t(167.95)= -4.28$, $p<.001$, $p\text{-adjust}<.001$
	Orbitofrontal prefrontal cortex	.138	.035	.147	.047	$t(168.57)= -1.46$, $p=.146$, $p\text{-adjust}= 2.044$
	Subgenual cingulate cortex	.195	.043	.134	.047	$t(171.19)= 8.92$, $p<.001$, $p\text{-adjust}<.001$
	Ventral striatum	.124	.040	.135	.037	$t(163.33)= -1.80$, $p=.073$, $p\text{-adjust}= 1.025$

2 ¹ p -values were Bonferroni-corrected for multiple 14 model comparisons

3

4 **Table S6.** Average path estimates for group- and subgroup-level connections

<i>Path type</i>	<i>Connection¹</i>	<i>N</i>	<i>Mean</i>	<i>SD</i>	<i>Max</i>	<i>Min</i>
Group	L. Amy – R. Amy	174	.412	.204	1.01	-.297
	L. dACC – R. dACC	174	.446	.267	1.03	-.604
	R. dmPFC – L. dmPFC	174	.414	.252	1.07	-.238
	R. Ins – L. Ins	174	.414	.245	.852	-.438
	L. Ins – L. dACC	174	.215	.213	.993	-.393
	R. OFC – R. sgACC	174	.394	.244	1.19	-1.03
	L. sgACC – L. OFC	174	.365	.257	1.36	-.546

	L. sgACC – R. VS	174	.253	.212	.897	-.557
	R. VS – L. VS	174	.478	.197	.891	-.376
Subgroup (A)	L. dmPFC – L. dACC	80	.223	.288	1.26	-.276
	R. OFC – L. OFC	80	.196	.319	.673	-1.16
	R. sgACC – L. Amyg	80	.103	.210	.531	-.494
	R. sgACC – L. sgACC	80	.355	.305	1.06	-.649
	R. sgACC – L. VS	80	.222	.201	.712	-.394
	L. VS – R. Ins	80	.182	.223	.747	-.313
	L. dmPFC – R. Ins	94	-.151	.199	.464	-.732
Subgroup (B)	R. Ins – R. dACC	94	.180	.186	.536	-.306
	L. OFC – R. OFC	94	.367	.200	.857	-.044

¹ L. and R. indicate left/right hemisphere; Amyg = amygdala; dACC = dorsal anterior cingulate;

dmPFC = dorsomedial prefrontal; Ins = insula; OFC = orbitofrontal; sgACC = subgenual

cingulate; VS = ventral striatum

Table S7. Results from predictive models predicting anxiety and depressive symptoms including

all covariates

Model: Change in symptoms (slope) ~ subgroup + initial symptoms (intercept) + all covariates

	Change in anxiety		Change in depression	
	β	p	β	p
Subgroup	0.257	0.011	0.145	0.182
Initial symptoms	-0.315	0.002	0.119	0.246
Male	0.099	0.427	0.248	0.067
Puberty	0.076	0.525	0.024	0.853
Age	0.127	0.172	0.010	0.919
White	0.211	0.037	-0.019	0.860
Hispanic	0.081	0.391	0.151	0.142
Other	-0.114	0.211	-0.102	0.305
Baseline income	0.012	0.902	0.109	0.318
Pandemic duration	0.012	0.899	-0.077	0.461
Motion	-0.082	0.394	0.002	0.987
Violence exposure	0.004	0.968	0.032	0.784
Social deprivation	0.057	0.598	-0.068	0.563
Reading comprehension	0.171	0.146	0.158	0.218
Math abilities	-0.045	0.707	0.074	0.574
Living w/ partner	0.142	0.124	0.131	0.198
Living w/ child	0.194	0.040	0.139	0.179
	$F(17,92)=2.68, p=.001$		$F(17,92)=1.35, p=.178$	

- 1 Model: Symptoms during pandemic ~ subgroup * COVID-19 economic adversity + initial level
 2 of symptom + all covariates

	Anxiety at wave 3		Depression at wave 3	
	β	p	β	p
Subgroup	0.238	0.007	0.037	0.624
COVID-19 adversity	0.133	0.263	0.030	0.771
Subgroup x COVID-19 adversity	0.259	0.031	0.145	0.160
Initial symptoms	0.406	0.000	0.735	0.000
Male	0.024	0.827	0.084	0.362
Puberty	0.039	0.705	-0.051	0.569
Age	0.109	0.184	-0.030	0.674
White	0.247	0.005	0.007	0.921
Hispanic	0.096	0.241	0.139	0.052
Other	-0.041	0.604	-0.003	0.966
Baseline income	0.021	0.816	0.041	0.602
Pandemic duration	0.030	0.726	-0.011	0.881
Motion	-0.146	0.094	-0.036	0.628
Violence exposure	-0.087	0.374	-0.025	0.763
Social deprivation	0.093	0.324	-0.036	0.660
Reading comprehension	0.147	0.157	0.098	0.280
Math abilities	-0.075	0.480	0.028	0.762
Living w/ partner	0.113	0.164	0.058	0.407
Living w/ child	0.105	0.228	0.052	0.486
	$F(19,89)=4.90, p<.001$		$F(19,88)=8.20, p<.001$	

- 3
 4 **Table S8.** Individual node centrality predicting change in symptoms, adjusting for initial levels
 5 (tested in separate models)

Models / Predictor	Change in anxiety			Change in depression		
	β	p	p_{adjust}	β	p	p_{adjust}
L. Amygdala	.042	.536	7.504	.042	.585	8.19
R. Amygdala	-.049	.478	6.692	-.188	.013	.182
L. Dorsal anterior cingulate	.058	.396	5.544	.043	.578	8.092
R. Dorsal anterior cingulate	-.030	.666	9.324	.022	.777	10.878
L. Dorsomedial prefrontal	.059	.386	5.404	.084	.272	3.808
R. Dorsomedial prefrontal	-.018	.796	11.144	.072	.345	4.83
L. Insula	-.022	.753	10.542	.047	.539	7.546
R. Insula	-.106	.120	1.69	-.205	.007	.098
L. Orbitofrontal	-.018	.799	11.186	.105	.170	2.38
R. Orbitofrontal	-.016	.813	11.382	.004	.958	13.412
L. Subgenual cingulate	-.055	.425	5.95	-.151	.048	.672

R. Subgenual cingulate	.160	.019	.266	.124	.103	1.442
L. Ventral striatum	.085	.213	2.982	.026	.733	10.262
R. Ventral striatum	-.164	.016	.224	-.063	.409	5.726

Table S9. Comparison between extracted data using 4mm-radii node spheres and 6.5mm-radii node spheres

Region	Mean (SD) (8mm-diameter)	Mean (SD) (6.5mm-radii)	t-test results
Left Amygdala	6785.061 (781.231)	6749.546 (704.276)	$t(346)=.445, p=.657$
Right Amygdala	7294.925 (885.737)	7205.825 (783.190)	$t(346)=.995, p=.320$

Table S10. Results from split-half reliability test ($N=174$)

GIMME subgroups	Count (%)	Path (non-lagged) count M (SD)
Subgroup A	Odd = 73 (41.95%) Even = 67 (38.51%)	Odd = 29.00 (5.68) Even = 24.75 (6.44)
Subgroup B	Odd = 101 (58.05%) Even = 107 (61.49%)	Odd = 28.70 (3.82) Even = 24.56 (4.40)

	Subgroup A	Subgroup B
Odd	73	101
Even	67	107

$\chi^2(1)=0.299, p=.585$

Table S11. Results from 80% randomly drawn subsample test

Sample	Subgroup membership ¹ Count (%)	Path (non-lagged) ¹ M (SD)	Anxiety comparison with full sample
Full sample ($N=174$)	A = 80 (45.98%) B = 94 (54.02%)	A = 32.4 (4.69) B = 27.0 (3.62)	N/A
Subsample 1 ($N=139$)	A = 60 (43.17%) B = 79 (56.83%)	A = 32.0 (4.95) B = 27.4 (3.75)	$t(89)=-.400, p=.690$ $t(119)=.090, p=.929$
Subsample 2 ($N=139$)	A = 69 (49.64%) B = 70 (50.36%)	A = 33.3 (4.57) B = 26.9 (3.64)	$t(98)=-.027, p=.979$ $t(110)=.004, p=.997$
Subsample 3 ($N=139$)	A = 76 (54.68%) B = 63 (45.32%)	A = 32.8 (5.06) B = 27.1 (3.51)	$t(102)=-.367, p=.714$ $t(110)=.213, p=.832$
Subsample 4 ($N=139$)	A = 55 (39.57%) B = 84 (60.43%)	A = 35.5 (4.50) B = 26.8 (3.39)	$t(88)=.181, p=.857$ $t(121)=.551, p=.583$

Subsample 5 (<i>N</i> =139)	A = 65 (46.76%) B = 74 (53.24%)	A = 34.0 (4.40) B = 27.1 (3.58)	<i>t</i> (95)=.146, <i>p</i> =.884 <i>t</i> (117)=.046, <i>p</i> =.963
---------------------------------	------------------------------------	------------------------------------	---

1

2 Chi-square test results comparing subgroup membership of original sample and subsamples

	Subgroup A	Subgroup B
Subgroup membership in original sample	62	77
Subgroup membership in Subsample 1	60	79

3 $\chi^2(1) = .015, p = .904$

Subgroup membership in original sample	69	70
Subgroup membership in Subsample 2	69	70

4 $\chi^2(1) = 1, p = 1$

Subgroup membership in original sample	67	72
Subgroup membership in Subsample 3	76	63

5 $\chi^2(1) = .922, p = .337$

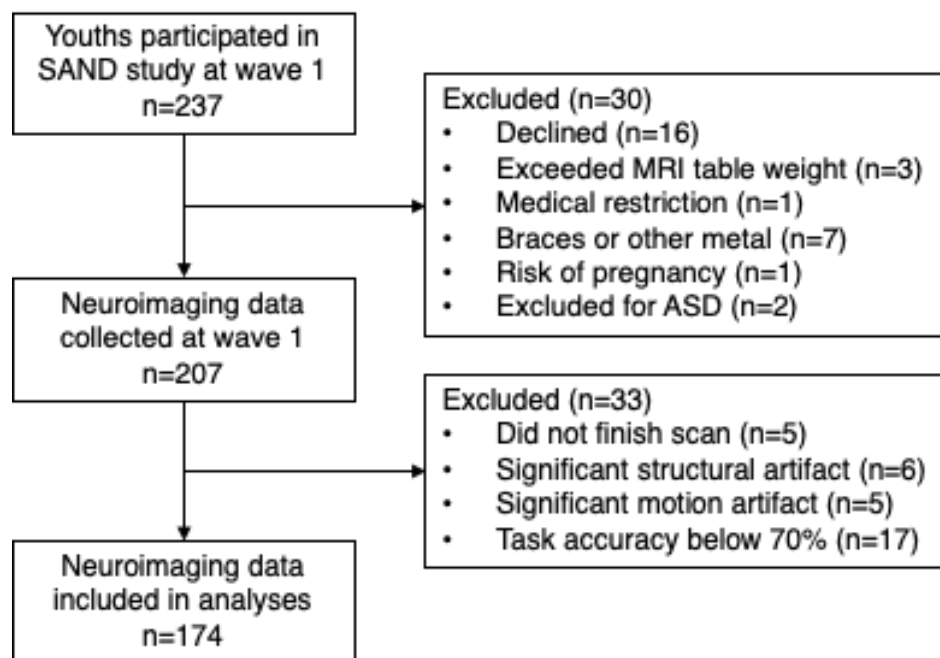
Subgroup membership in original sample	63	76
Subgroup membership in Subsample 4	55	84

6 $\chi^2(1) = .722, p = .396$

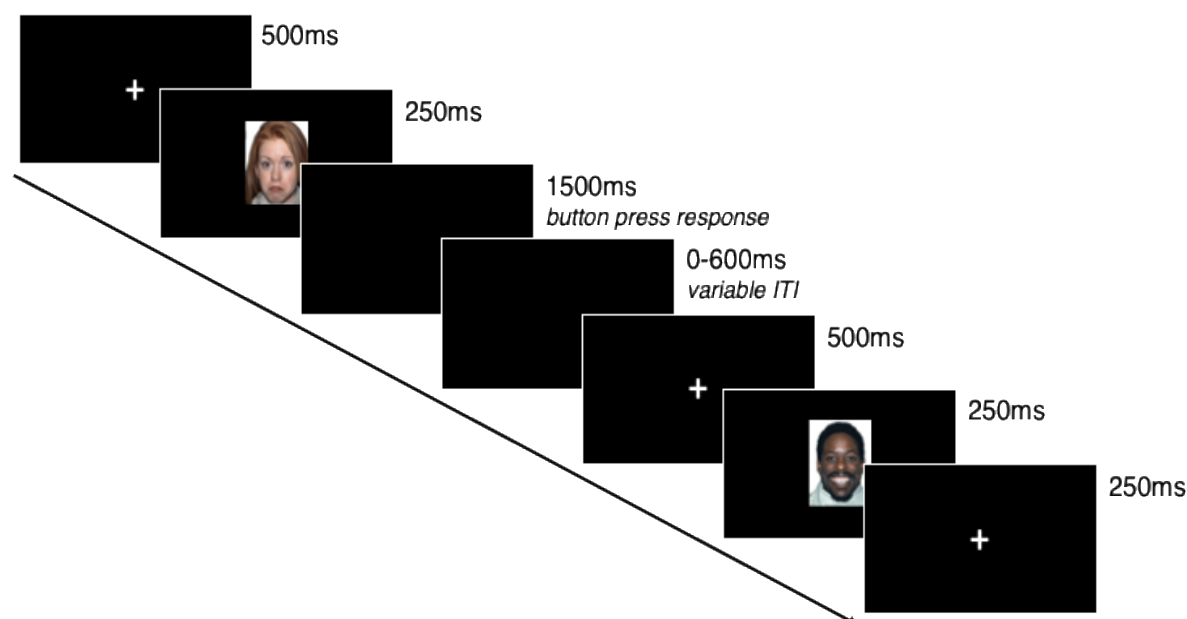
Subgroup membership in original sample	65	74
Subgroup membership in Subsample 5	65	74

7 $\chi^2(1) = 1, p = 1$

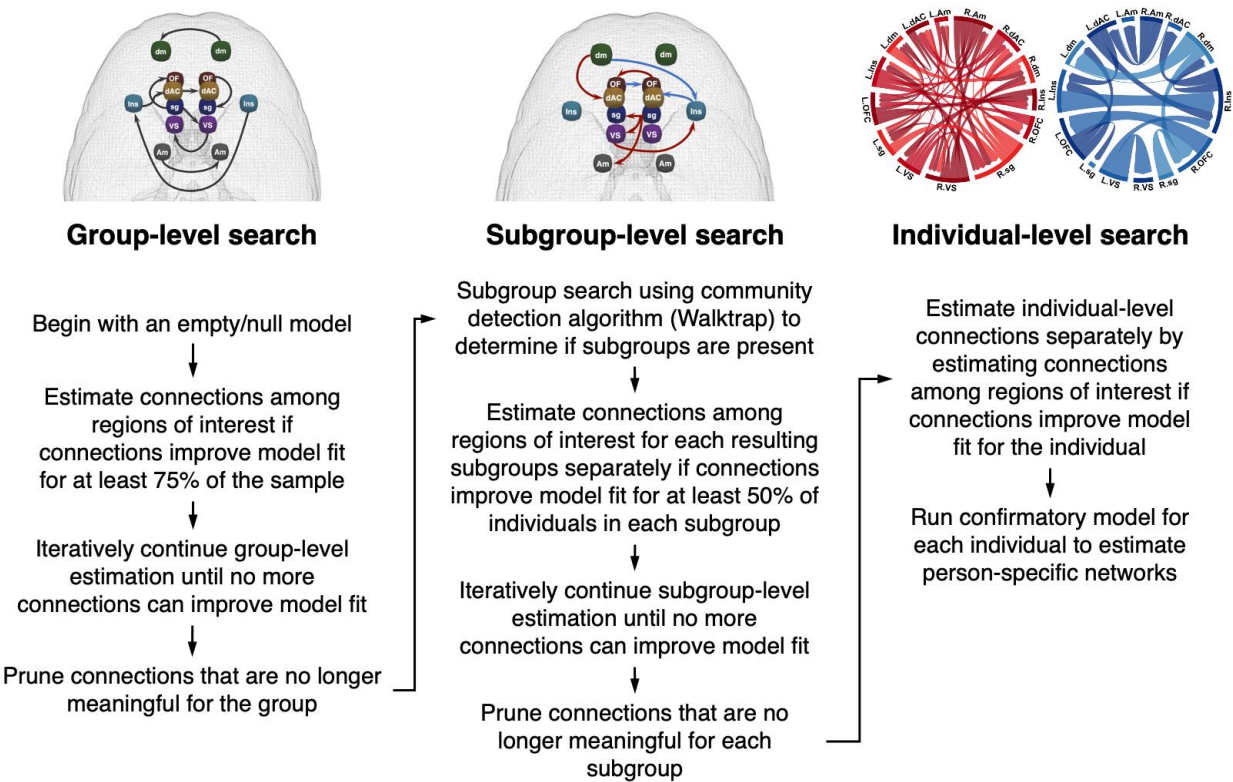
1 **Figure S1.** Exclusionary criteria for neuroimaging data



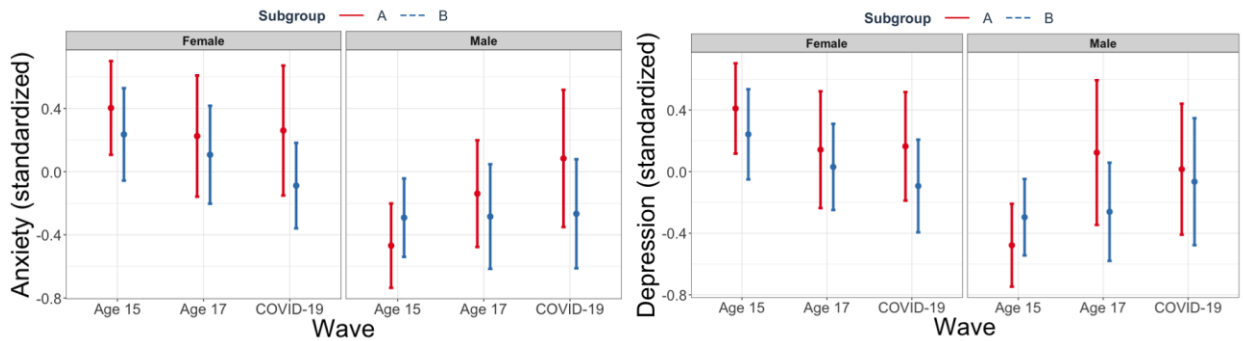
4 **Figure S2.** fMRI task paradigm



1 **Figure S3.** S-GIMME flowchart



2
3
4 **Figure S4.** Anxiety and depression for each subgroup, stratified by sex

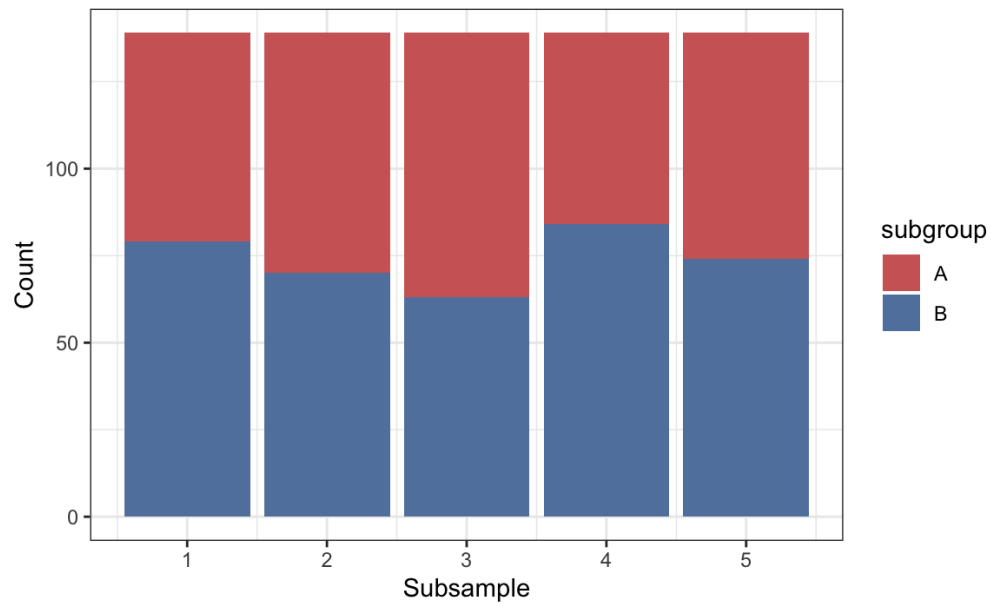


5
6 Anxiety and depression for each subgroup stratified by sex. Sex differences in both anxiety and
7 depression were most pronounced at adolescence (age 15) where females were reporting greater
8 symptoms, especially those with denser network profiles. Observed sex differences were
9 markedly diminished during COVID-19 for both subgroups. Both males and females with

1 Subgroup A denser network profiles (in red) showed greater anxiety symptoms during COVID-
2 19 compared to Subgroup B (in blue). Each point represents mean value and the bars indicate
3 standard errors.

4

5 **Figure S5.** GIMME results based on 5 randomly drawn 80% subsamples



6

References

- Adriene M. Beltz, Hailey L. Dotterer, & Leigh G. Goetschius. (2019). *GIMME Preprocessing: Initial Release*. Zenodo. <https://doi.org/10.5281/zenodo.2692522>
- Angold, A., Costello, E. J., Messer, S. C., & Pickles, A. (1995). Development of a short questionnaire for use in epidemiological studies of depression in children and adolescents. *International Journal of Methods in Psychiatric Research*, 5(4), 237–249.
- Beck, A. T., Epstein, N., Brown, G., & Steer, R. A. (1988). An inventory for measuring clinical anxiety: Psychometric properties. *Journal of Consulting and Clinical Psychology*, 893–897.
- Beck, A. T., Steer, R. A., & Brown, G. (1996). *Beck Depression Inventory–II* (Vol. 10). Pearson.
- Birmaher, B., Khetarpal, S., Brent, D., Cully, M., Balach, L., Kaufman, J., & Neer, S. M. (1997). The Screen for Child Anxiety Related Emotional Disorders (SCARED): Scale construction and psychometric characteristics. *Journal of the American Academy of Child and Adolescent Psychiatry*, 36(4), 545–553. <https://doi.org/10.1097/00004583-199704000-00018>
- Davidson, R. J. (2002). Anxiety and affective style: Role of prefrontal cortex and amygdala. *Biological Psychiatry*, 51(1), 68–80. [https://doi.org/10.1016/S0006-3223\(01\)01328-2](https://doi.org/10.1016/S0006-3223(01)01328-2)
- Davis, M. (1992). The role of the amygdala in fear and anxiety. *Annual Review of Neuroscience*, 15(1), 353–375.
- Drevets, W. C. (2007). Orbitofrontal Cortex Function and Structure in Depression. *Annals of the New York Academy of Sciences*, 1121(1), 499–527. <https://doi.org/10.1196/annals.1401.029>

- 1 Drevets, W. C., Savitz, J., & Trimble, M. (2008). The Subgenual Anterior Cingulate Cortex in
2 Mood Disorders. *CNS Spectrums*, 13(8), 663–681.
- 3 Eickhoff, S. B., Laird, A. R., Fox, P. T., Bzdok, D., & Hensel, L. (2016). Functional Segregation
4 of the Human Dorsomedial Prefrontal Cortex. *Cerebral Cortex*, 26(1), 304–321.
5 <https://doi.org/10.1093/cercor/bhu250>
- 6 Elliott, M. L., Knodt, A. R., & Hariri, A. R. (2021). Striving toward translation: Strategies for
7 reliable fMRI measurement. *Trends in Cognitive Sciences*, 25(9), 776–787.
8 <https://doi.org/10.1016/j.tics.2021.05.008>
- 9 Gates, K. M., Lane, S. T., Varangis, E., Giovanello, K., & Guiskewicz, K. (2017). Unsupervised
10 Classification During Time-Series Model Building. *Multivariate Behavioral Research*,
11 52(2), 129–148. <https://doi.org/10.1080/00273171.2016.1256187>
- 12 Gates, K. M., Molenaar, P. C. M., Hillary, F. G., Ram, N., & Rovine, M. J. (2010). Automatic
13 search for fMRI connectivity mapping: An alternative to Granger causality testing using
14 formal equivalences among SEM path modeling, VAR, and unified SEM. *NeuroImage*,
15 50(3), 1118–1125. <https://doi.org/10.1016/j.neuroimage.2009.12.117>
- 16 Glover, G. H., & Law, C. S. (2001). Spiral-in/out BOLD fMRI for increased SNR and reduced
17 susceptibility artifacts. *Magnetic Resonance in Medicine*, 46(3), 515–522. Scopus.
18 <https://doi.org/10.1002/mrm.1222>
- 19 Goetschius, L. G., Hein, T. C., McLanahan, S. S., Brooks-Gunn, J., McLoyd, V. C., Dotterer, H.
20 L., Lopez-Duran, N., Mitchell, C., Hyde, L. W., Monk, C. S., & Beltz, A. M. (2020).
21 Association of Childhood Violence Exposure With Adolescent Neural Network Density.
22 *JAMA Network Open*, 3(9). <https://doi.org/10.1001/jamanetworkopen.2020.17850>

Goetschius, L. G., Hein, T. C., Mitchell, C., Lopez-Duran, N. L., McLoyd, V. C., Brooks-Gunn, J., McLanahan, S. S., Hyde, L. W., & Monk, C. S. (2020). Childhood violence exposure and social deprivation predict adolescent amygdala-orbitofrontal cortex white matter connectivity. *Developmental Cognitive Neuroscience*, 45, 100849.

<https://doi.org/10.1016/j.dcn.2020.100849>

Greicius, M. D., Flores, B. H., Menon, V., Glover, G. H., Solvason, H. B., Kenna, H., Reiss, A. L., & Schatzberg, A. F. (2007). Resting-State Functional Connectivity in Major Depression: Abnormally Increased Contributions from Subgenual Cingulate Cortex and Thalamus. *Biological Psychiatry*, 62(5), 429–437.

<https://doi.org/10.1016/j.biopsych.2006.09.020>

Hein, T. C., Goetschius, L. G., McLoyd, V. C., Brooks-Gunn, J., McLanahan, S. S., Mitchell, C., Lopez-Duran, N. L., Hyde, L. W., & Monk, C. S. (2020). Childhood violence exposure and social deprivation are linked to adolescent threat and reward neural function. *Social Cognitive and Affective Neuroscience*, 15(11), 1252–1259.

<https://doi.org/10.1093/scan/nsaa144>

Janak, P. H., & Tye, K. M. (2015). From circuits to behaviour in the amygdala. *Nature*, 517(7534), 284–292. <https://doi.org/10.1038/nature14188>

Jenkinson, M., Beckmann, C. F., Behrens, T. E. J., Woolrich, M. W., & Smith, S. M. (2012). FSL. *NeuroImage*, 62(2), 782–790. <https://doi.org/10.1016/j.neuroimage.2011.09.015>

Klumpp, H., Angstadt, M., & Phan, K. L. (2012). Insula reactivity and connectivity to anterior cingulate cortex when processing threat in generalized social anxiety disorder. *Biological Psychology*, 89(1), 273–276. <https://doi.org/10.1016/j.biopsycho.2011.10.010>

- 1 Klumpp, H., Post, D., Angstadt, M., Fitzgerald, D. A., & Phan, K. L. (2013). Anterior cingulate
2 cortex and insula response during indirect and direct processing of emotional faces in
3 generalized social anxiety disorder. *Biology of Mood & Anxiety Disorders*, 3(1), 1–9.
4 <https://doi.org/10.1186/2045-5380-3-7>
- 5 Lütkepohl, H. (2005). *New Introduction to Multiple Time Series Analysis*. Springer Science &
6 Business Media.
- 7 Margulies, D. S., Kelly, A. M. C., Uddin, L. Q., Biswal, B. B., Castellanos, F. X., & Milham, M.
8 P. (2007). Mapping the functional connectivity of anterior cingulate cortex. *NeuroImage*,
9 37(2), 579–588. <https://doi.org/10.1016/j.neuroimage.2007.05.019>
- 10 Mayberg, H. S., Lozano, A. M., Voon, V., McNeely, H. E., Seminowicz, D., Hamani, C.,
11 Schwalb, J. M., & Kennedy, S. H. (2005). Deep Brain Stimulation for Treatment-
12 Resistant Depression. *Neuron*, 45(5), 651–660.
13 <https://doi.org/10.1016/j.neuron.2005.02.014>
- 14 Menon, V., & Uddin, L. Q. (2010). Saliency, switching, attention and control: A network model
15 of insula function. *Brain Structure and Function*, 214(5–6), 655–667.
16 <https://doi.org/10.1007/s00429-010-0262-0>
- 17 Moses-Kolko, E. L., Perlman, S. B., Wisner, K. L., James, J., Saul, A. T., & Phillips, M. L.
18 (2010). Abnormally Reduced Dorsomedial Prefrontal Cortical Activity and Effective
19 Connectivity With Amygdala in Response to Negative Emotional Faces in Postpartum
20 Depression. *American Journal of Psychiatry*, 167(11), 1373–1380.
21 <https://doi.org/10.1176/appi.ajp.2010.09081235>

- 1 Pagnoni, G., Zink, C. F., Montague, P. R., & Berns, G. S. (2002). Activity in human ventral
2 striatum locked to errors of reward prediction. *Nature Neuroscience*, 5(2), 97–98.
3 <https://doi.org/10.1038/nn802>
- 4 Peckins, M. K., Roberts, A. G., Hein, T. C., Hyde, L. W., Mitchell, C., Brooks-Gunn, J.,
5 McLanahan, S. S., Monk, C. S., & Lopez-Duran, N. L. (2020). Violence exposure and
6 social deprivation is associated with cortisol reactivity in urban adolescents.
7 *Psychoneuroendocrinology*, 111, 104426.
8 <https://doi.org/10.1016/j.psyneuen.2019.104426>
- 9 Petersen, A. C., Crockett, L., Richards, M., & Boxer, A. (1988). A self-report measure of
10 pubertal status: Reliability, validity, and initial norms. *Journal of Youth and Adolescence*,
11 17(2), 117–133. <https://doi.org/10.1007/BF01537962>
- 12 Power, J. D., Barnes, K. A., Snyder, A. Z., Schlaggar, B. L., & Petersen, S. E. (2012). Spurious
13 but systematic correlations in functional connectivity MRI networks arise from subject
14 motion. *Neuroimage*, 59(3), 2142–2154.
15 <https://doi.org/10.1016/j.neuroimage.2011.10.018>
- 16 Pronk, T., Molenaar, D., Wiers, R. W., & Murre, J. (2022). Methods to split cognitive task data
17 for estimating split-half reliability: A comprehensive review and systematic assessment.
18 *Psychonomic Bulletin & Review*, 29(1), 44–54. [https://doi.org/10.3758/s13423-021-](https://doi.org/10.3758/s13423-021-01948-3)
19 01948-3
- 20 Rauch, S. L., Shin, L. M., & Wright, C. I. (2003). Neuroimaging Studies of Amygdala Function
21 in Anxiety Disorders. *Annals of the New York Academy of Sciences*, 985(1), 389–410.
22 <https://doi.org/10.1111/j.1749-6632.2003.tb07096.x>

- 1 Robinson, O. J., Cools, R., Carlisi, C. O., Sahakian, B. J., & Drevets, W. C. (2012). Ventral
2 Striatum Response During Reward and Punishment Reversal Learning in Unmedicated
3 Major Depressive Disorder. *American Journal of Psychiatry*, 169(2), 152–159.
4 <https://doi.org/10.1176/appi.ajp.2011.11010137>
- 5 Schultz, W., Apicella, P., Scarnati, E., & Ljungberg, T. (1992). Neuronal activity in monkey
6 ventral striatum related to the expectation of reward. *Journal of Neuroscience*, 12(12),
7 4595–4610. <https://doi.org/10.1523/JNEUROSCI.12-12-04595.1992>
- 8 Smith, S. M. (2012). The future of fMRI connectivity. *NeuroImage*, 62(2), 1257–1266.
9 <https://doi.org/10.1016/j.neuroimage.2012.01.022>
- 10 Stevens, F. L., Hurley, R. A., Taber, K. H., Hurley, R. A., Hayman, L. A., & Taber, K. H.
11 (2011). Anterior Cingulate Cortex: Unique Role in Cognition and Emotion. *The Journal*
12 *of Neuropsychiatry and Clinical Neurosciences*, 23(2), 121–125.
13 <https://doi.org/10.1176/jnp.23.2.jnp121>
- 14 Straus, M. A., Hamby, S. L., Finkelhor, D., Moore, D. W., & Runyan, D. (1998). Identification
15 of Child Maltreatment With the Parent-Child Conflict Tactics Scales: Development and
16 Psychometric Data for a National Sample of American Parents. *Child Abuse & Neglect*,
17 22(4), 249–270. [https://doi.org/10.1016/S0145-2134\(97\)00174-9](https://doi.org/10.1016/S0145-2134(97)00174-9)
- 18 Thomas, K. M., Drevets, W. C., Dahl, R. E., Ryan, N. D., Birmaher, B., Eccard, C. H., Axelson,
19 D., Whalen, P. J., & Casey, B. J. (2001). Amygdala Response to Fearful Faces in
20 Anxious and Depressed Children. *Archives of General Psychiatry*, 58(11), 1057–1063.
21 <https://doi.org/10.1001/archpsyc.58.11.1057>
- 22 Tottenham, N., Tanaka, J. W., Leon, A. C., McCarry, T., Nurse, M., Hare, T. A., Marcus, D. J.,
23 Westerlund, A., Casey, B. J., & Nelson, C. (2009). The NimStim set of facial

- expressions: Judgments from untrained research participants. *Psychiatry Research*,
168(3), 242–249. <https://doi.org/10.1016/j.psychres.2008.05.006>
- Uddin, L. Q. (2015). Salience processing and insular cortical function and dysfunction. *Nature
Reviews Neuroscience*, 16(1), 55–61. <https://doi.org/10.1038/nrn3857>
- Whalen, P. J., Shin, L. M., Somerville, L. H., McLean, A. A., & Kim, H. (2002). Functional
neuroimaging studies of the amygdala in depression. *Seminars in Clinical
Neuropsychiatry*, 7(4), 234–242. <https://doi.org/10.1053/scnp.2002.35219>
- Woodcock, R. W., McGrew, K. S., & Mather, N. (2001). *Woodcock-Johnson III tests of
achievement*.
- Woolrich, M. W., Ripley, B. D., Brady, M., & Smith, S. M. (2001). Temporal autocorrelation in
univariate linear modeling of FMRI data. *NeuroImage*, 14(6), 1370–1386.
<https://doi.org/10.1006/nimg.2001.0931>
- Yarkoni, T., Poldrack, R. A., Nichols, T. E., Van Essen, D. C., & Wager, T. D. (2011). Large-
scale automated synthesis of human functional neuroimaging data. *Nature Methods*, 8(8),
665–670. <https://doi.org/10.1038/nmeth.1635>